THE JOURNAL OF PHYSICAL CHEMISTRY B

Article

pubs.acs.org/JPCB

Engineering Interface Structure to Improve Efficiency and Stability of Organometal Halide Perovskite Solar Cells

Longbin Qiu, Luis K. Ono, Yan Jiang, Matthew R. Leyden, Sonia R. Raga, Shenghao Wang, and Yabing Qi*

Energy Materials and Surface Sciences Unit (EMSS), Okinawa Institute of Science and Technology Graduate University (OIST), 1919-1 Tancha, Onna-son, Kunigami-gun, Okinawa 904-0495, Japan

Supporting Information

ABSTRACT: The rapid rise of power conversion efficiency (PCE) of low cost organometal halide perovskite solar cells suggests that these cells are a promising alternative to conventional photovoltaic technology. However, anomalous hysteresis and unsatisfactory stability hinder the industrialization of perovskite solar cells. Interface engineering is of importance for the fabrication of highly stable and hysteresis free perovskite solar cells. Here we report that a surface modification of the widely used TiO_2 compact layer can give insight into interface interaction in perovskite solar cells. A highest PCE of 18.5% is obtained using anatase TiO_2, but the device is not stable and degrades rapidly. With an amorphous TiO_2 compact layer, the devices show a prolonged lifetime but a lower PCE and more pronounced hysteresis. To achieve a high PCE and long lifetime simultaneously, an insulating polymer interface layer is deposited on top of TiO_2. Three polymers, each with a different functional group (hydroxyl, amino, or aromatic group), are investigated to further understand the relation of interface structure and device PCE as well as stability. We show that it is necessary to consider not only the band alignment at the interface, but also interface chemical interactions between the thin interface layer and the perovskite film. The hydroxyl and amino groups interact with $CH_3NH_3PbI_3$ leading to poor PCEs. In contrast, deposition of a thin layer of polymer consisting of an aromatic group to prevent the direct contact of TiO_2 and $CH_3NH_3PbI_3$ can significantly enhance the device stability, while the same time maintaining a high PCE. The fact that a polymer interface layer on top of TiO_2 can enhance device stability, strongly suggests that the interface interaction between TiO_2 and $CH_3NH_3PbI_3$ plays a crucial role. Our work highlights the importance of interface structure and paves the way for further optimization of PCEs and stability of perovskite solar cells.

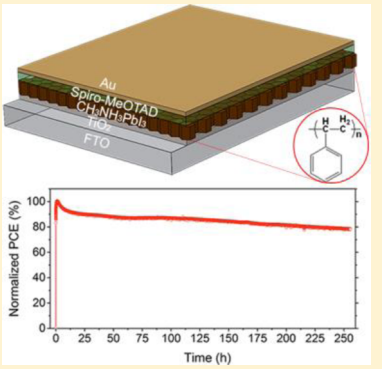

INTRODUCTION

Highly efficient perovskite solar cells (PSCs) have attracted great interest due to their potential as a low cost alternative to traditional silicon solar cells. The power conversion efficiency (PCE) of PSCs increased from 3.8% to over 20% in just 6 years.[1−3] However, the anomalous hysteresis and poor stability hinder the industrialization of perovskite-based devices. Stability issues can be attributed mainly to three factors. The first factor is the perovskite active layer itself.[4] To improve the stability of PSCs, mixed cation and/or halide perovskites have been synthesized, and these mixed cations or halide ions can stabilize the structure, and thus enhance stability under operation.[5−8] The second factor influencing device stability of PSCs is the choice of other layers in PSCs, including bottom/top electrodes,[9] hole transporting layers (HTLs),[10−12] and electron transport layers (ETLs).[13,14] The third factor of importance for stable PSCs is the interface at the bottom/top of the perovskite active layer.[15] The interface layer might interact with the active layer, and trapped charges at interfaces can induce the degradation of PSCs.[16] In addition, the presence of interface trap states has been proposed to be one of the main causes for the anomalous hysteresis effect.[17,18] Furthermore, recombination at the interface between the charge extraction layer and perovskite layer is reported to be more dominant than that at grain boundaries.[19]

The TiO_2 ETL is commonly used in PSCs, and is a low cost and promising option for high performance devices.[20] PSCs based on TiO_2 ETL often show anomalous hysteresis.[21] To address the hysteresis/stability problems of TiO_2, surface modification,[22] metallic ion doping,[23,24] surface passivation with chloride,[25] have been investigated. In addition, many alternatives, such as SnO_2, ZnO, and PCBM[26−28] have been investigated. However, in many cases the better performing devices are still the ones using TiO_2 ETL, and the alternatives often cause other problems. For example, ZnO can degrade the perovskite active layer and is not suitable for stable PSCs.[14] Although many modifications to TiO_2 have been shown to improve the performance of PSCs, it is still inconclusive how the structures/properties of the compact layer influence the performance of PSCs. There are a number of reports

Special Issue: Miquel B. Salmeron Festschrift

Received: April 26, 2017
Revised: May 11, 2017
Published: May 17, 2017

DOI: 10.1021/acs.jpcb.7b03921
J. Phys. Chem. B XXXX, XXX, XXX−XXX

investigating the intrinsic properties of the TiO_2/perovskite interface. For instance, defective anatase TiO_2 has been reported to lead to higher performance.[29] Trapped charges at the interface between perovskite and TiO_2 can cause both anomalous hysteresis and degradation.[16] Furthermore, the photocatalytic activity of TiO_2 can degrade the perovskite active layer under ultraviolet illumination.[30,31] To eliminate the stability issue of PSCs that comes from ultraviolet illumination on TiO_2 ETL, a photocurable fluoropolymer that functions as ultraviolet absorption coating has been studied.[32] With an ultraviolet cutoff filter the solar cell operates at maximum power output point for more than 500 h retaining 95% of its initial PCE.[25] However, this filter will lower the absorption of incident light. Engineering the interface to achieve both high PCE and stability of PSCs remains a grand challenge.

In this work, we demonstrate that the structure of TiO_2 is important for the PCE and stability of PSCs. The performance of a planar structure solar cell has a PCE higher than 18% using crystalline TiO_2 and shows less hysteresis than amorphous TiO_2 with a PCE of approximately 17%. However, the PCE of PSCs based on crystalline TiO_2 ETL drops much faster than that of PSCs based on amorphous TiO_2 ETL. Without the TiO_2 compact layer the device exhibits even better stability, but the PCE is significantly lower (usually <14%). Based on these observations, we conclude that it is the direct contact interaction between TiO_2 and $CH_3NH_3PbI_3$ that causes the PCE deterioration. We propose an insulating polymer interface layer for surface modification of TiO_2. Polyethylenimine ethoxylated (PEIE), polyethylenimine (PEI), and polystyrene (PS), consisting of hydroxyl, amino and aromatic groups, respectively, are chosen as three candidate polymers. A thin polymer layer as a tunneling layer can suppress the interaction between TiO_2 and perovskite layer.[33] We find that a PEIE or PEI layer causes the solar cell PCE to decrease significantly. Here the polar functional groups, such as hydroxyl and amino groups, might have a negative effect on $CH_3NH_3PbI_3$ and therefore are not suitable as modifiers. With a PS layer the solar cell PCE does not show much decrease, and more importantly it exhibits a prolonged lifetime. In dry N_2 the solar cell is stable for more than 250 h under the continuous operation at the maximum power point.

EXPERIMENTAL SECTION

Fabrication of Solar Cells. Patterned FTO substrates were first washed sequentially in 1 wt% sodium dodecyl sulfate solution, water, isopropanol, and acetone using an ultrasonicator. Before use, the FTO substrates were treated with UV-Ozone for 15 min. Amorphous TiO_2 was deposited with a radio frequency sputtering technique (Vacuum Sputter Deposition System, CAM-S, ULVAC) in a condition of 10 sccm Ar with a power of 180 W for 45 min. Sintered compact TiO_2 layer was fabricated by annealing the amorphous sputtered TiO_2 thin film at 500 °C. PEIE (polyethylenimine, 80% ethoxylated solution, 35−40 wt% in H_2O, Mw ∼ 70000) and PEI (branched, Mw ∼ 25000) was purchased from Sigma-Aldrich and diluted with methoxyethanol. For PEIE and PEI layers the solution was spun onto TiO_2 at 5000 rpm for 60 s. Polystyrene was purchase from Aldrich (Mw ∼ 350 000) and dissolved into o-dichlorobenzene with a concentration of 0.2 mg/mL. The solution of $CH_3NH_3PbI_3$ (1.2 M) was made by mixing PbI_2 (TCI) and CH_3NH_3I (dyesol) into a DMF and DMSO mixed solvent (v/v = 7/1). For the $CH_3NH_3PbI_3$ layer, a 20 μL solution was cast onto substrates and spin coated at 2800 rpm for 25 s. After 10 s of spinning, 200 μL of diethyl ether was drop cast onto the film. The $CH_3NH_3PbI_3$ film was formed after annealing at 100 °C for 60 min in 5% humidity.[34−36] A hole transport material solution (29 mg of spiro-MeOTAD (2,2′,7,7′-tetrakis (*N*,*N*-di-*p*-methoxyphenylamine)-9,9-spirobifluorene), 7 μL of lithium bis(trifluoromethylsulfonyl) imide solution (520 mg/mL in acetonitrile), and 11.5 μL of 4-*tert*-butylpyridine in 400 μL chlorobenzene) was spin coated at 3000 rpm for 30 s on top of $CH_3NH_3PbI_3$ film. Finally, a 70 nm thick Au film was deposited to complete the solar cell.

Characterization. The thickness of the amorphous TiO_2 layer and perovskite active layer was measured with a surface profiler (Bruker Dektak XT). The transmittance and absorbance spectra were measured with a UV−vis spectrometer (Jasco V-670). The surface morphology and element distribution characterization was performed in a scanning electron microscope (FEI Quanta 250 FEG). The ultraviolet photoemission spectroscopy (UPS) and X-ray photoelectron spectroscopy (XPS) spectra were recorded from an X-ray photoelectron spectrometer (XPS-AXIS Ultra HAS, Kratos) equipped with monochromatic Al−Kα = 1486.6 eV and nonmonochromatic He−I = 21.22 eV sources. UV and X-ray induced sample damage was monitored by taking five consecutive scans and by comparing these spectra. Crystal structure of TiO_2 and $CH_3NH_3PbI_3$ was characterized with an X-ray diffractometer (XRD) (Bruker D8 Discover). *J*−*V* curves were recorded by a Keithley 2420 source meter under illumination (100 mW/cm^2) of simulated AM1.5 solar light coming from a solar simulator (Oriel-Sol1A equipped with a 140 W Xe lamp and an AM1.5 filter). The light intensity was calibrated using a reference Si solar cell. The effective area of 0.1 cm^2 was defined by a mask. For stability measurements, the devices were operated at maximum power output under continuous one sun illumination. A customized software was used to record the maximum power output voltage and current every 5 s. The devices were kept at the maximum power output voltage during the intervals between consecutive measurements. No UV-filters were used, i.e., the UV component is included while under illumination. The stability measurement was performed either in ambient air with a relative humidity (RH) of 45% or in a nitrogen box with a RH below 5%. The EQE spectra were characterized by an IPCE measurement system (Oriel IQE 200).

RESULTS AND DISCUSSION

A planar structure in Figure 1a is used to fabricate PSCs in this work. Compact TiO_2 and spiro-MeOTAD are used as ETL and HTL, respectively. To understand how the TiO_2 structure will influence the solar cell PCE and stability, both crystalline and amorphous TiO_2 compact layers are used. Due to the ambipolar properties of $CH_3NH_3PbI_3$, the perovskite itself can transport both electrons and holes, which makes ETL-free or HTL-free devices possible.[37−39] ETL-free devices were fabricated as control samples. On the top of FTO glass we first sputtered a thin layer (thickness ∼40 nm (Figure S1)) of amorphous TiO_2. As comparison, the crystalline anatase TiO_2 samples were prepared by annealing the sputtered film at 500 °C for 30 min (Figure 1b). The XRD peak at 25.3° appearing after annealing is ascribed to the (101) diffraction plane of anatase TiO_2 (JCPDS No.: 84-1286).[40] To further investigate the structure/performance relation, a thin polar or nonpolar

DOI: 10.1021/acs.jpcb.7b03921
J. Phys. Chem. B XXXX, XXX, XXX−XXX

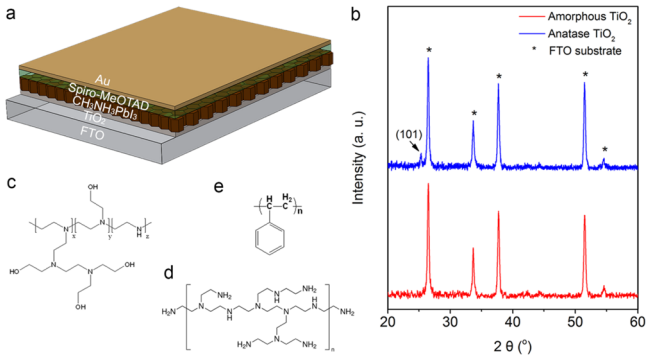

Figure 1. Solar cell structure and components. (a) Schematic drawing of a planar structure perovskite solar cell device. (b) XRD spectrum of amorphous and anatase TiO_2 compact layer. Molecular structure of (c) polyethylenimine ethoxylated (PEIE), (d) polyethylenimine (PEI), and (e) polystyrene (PS).

polymer modifier layer are introduced (Figure 1c–e) and will be discussed in the following section.

The photovoltaic performance for substrates with or without TiO_2 ETL is summarized in Figure 2a and Table 1. With a bare FTO substrate, the solar cells show an average PCE of 12.3%. All three photovoltaic parameters (i.e., open-circuit voltage V_{OC}, short-circuit current density J_{SC}, and fill factor FF) of the ETL-free devices are lower than those of the devices with TiO_2 ETL. With the introduction of amorphous TiO_2, a significant increase in J_{SC} is observed. Due to the higher electron selecting and hole blocking properties of the added TiO_2 layer, V_{OC} and FF also increase. This amorphous TiO_2 behaves surprisingly well achieving an average PCE of 16.4%. After annealing, the amorphous TiO_2 converts to crystalline anatase TiO_2 with a higher electron mobility.[40,41] The highest PCE of 18.5% is obtained, and the average PCE is 17.7%. Figure 2b clearly reveals the difference in photovoltaic parameters for these three kinds of devices. The most significant difference between anatase and amorphous TiO_2 is an increase in V_{OC}, which is consistent with calculated results that the crystal structure of TiO_2 affects the interface interaction and charge separation process.[42,43] However, the solar cells based on the crystalline anatase TiO_2 ETL show significantly worse stability than those based on the amorphous TiO_2 ETL. For example, in ambient conditions with a relative humidity (RH) of ~45%, the maximum power point tracking (MPPT) measurement shows almost no loss of PCE after operation for 1 h for the solar cell based on amorphous TiO_2 ETL (Figure 2c). For the anatase TiO_2 ETL-based device the PCE remains only ~80% after 1 h MPPT. Although the solar cells based on amorphous TiO_2 ETL show better stability, the lifetime is still relatively short and need further improvement. Device based on amorphous TiO_2 shows a T80 lifetime of 60 h with MPPT in a condition with RH of 5% (Figure S2).

Our experiment exhibits that devices based on the anatase TiO_2 ETL show decreased hysteresis compared to the devices based on the amorphous TiO_2 ETL (Figure 3a,b). Here the hysteresis is defined as the PCE difference between reverse scan and forward scan (Figure 3c). For planar structure PSCs based on TiO_2 ETL, hysteresis is commonly observed.[21] The hysteresis might decrease with a lower density of defects and trap states at the interface, as illustrated in PSCs based on SnO_2 ETL.[44] Also the higher electron extraction efficiency of anatase TiO_2 can contribute to decreased hysteresis.[29] Compared with the PSCs based on amorphous TiO_2 ETL, the PSCs based on crystalline anatase TiO_2 ETL show on average 2% lower hysteresis, which is consistent with the reported study that lower interface trap states help reduce hysteresis.[17]

To understand the influences of different TiO_2 ETLs (i.e., amorphous or anatase structure) on the PCE and stability, we first performed conductivity measurement on both TiO_2 ETLs. The thickness of TiO_2 is around 40 nm (Figure S1). Note that the thickness of TiO_2 used in this work is substantially smaller than the TiO_2 thickness in many reports (e.g., ~ 70 nm),[45,46] which we believe is part of the reason why perovskite solar cell performance is not so sensitively dependent on crystallinity of the TiO_2 electron transport layer. The conductivity of amorphous TiO_2 and anatase TiO_2 are 3.0×10^{-4} S/cm and 6.6×10^{-4} S/cm, respectively. The conductivity of anatase TiO_2 is indeed higher than that of amorphous TiO_2, but the difference can still be considered to be gentle enough (well below an order of magnitude). Therefore, on one hand, it would be reasonable to expect a slightly higher performance for perovskite solar cells based on anatase TiO_2, which is consistent with what we found. On the other hand, such a difference did not translate to a huge difference in perovskite solar cell performance. In fact, the high density of oxygen vacancies in amorphous TiO_2 can lead to similar conductivities measured in anatase TiO_2 nanocrystals (5.1×10^{-4} S/cm) or show even higher conductivities than the traditional high temperature spray coated TiO_2 (0.1×10^{-4} S/cm).[47−49] This high conductivity makes room temperature sputtered TiO_2 as a promising electron transport layer for high performance perovskite solar cell applications.

We further performed UPS and XPS measurement on amorphous and anatase TiO_2 ETLs (Figure 4). To be consistent with the device fabrication process, the TiO_2 coated substrates were treated with UV-Ozone for 15 min prior to UPS/XPS measurements. We measured several batches of samples, and the results are consistent and reproducible. The work function of anatase TiO_2 is ~0.2 eV lower than that of amorphous TiO_2 (Figure 4a). Assuming vacuum level alignment, the conduction band minimum (CBM) of anatase TiO_2 is higher than amorphous TiO_2, which might lead to a higher V_{OC} because of better matching with perovskite CBM.[50] The calculated atomic ratios suggest that both compact layers are oxygen deficient at the surface (Figure 4c,d and Table S1). The amorphous TiO_2 has more hydroxyl groups (associated with the peak around 532 eV) on the surface according to the fitting of O 1s core level spectrum (Figure 4d). The surface Ti−OH groups might induce tail states, change the electronic structure and further induce the localized band bending (Figure 4b).[51] These properties associated with amorphous TiO_2 are likely responsible for the still relatively low lifetime obtained for PSCs based on amorphous TiO_2 ETL. It is known that anatase TiO_2 is an efficient photocatalyst under UV-light and this is one of the reasons for the degradation of $CH_3NH_3PbI_3$ thus poor stability of perovskite solar cells. For anatase TiO_2, the higher degree of crystallinity leads to more severe photocatalytic interaction between the perovskite layer and anatase TiO_2, that would further accelerate the degradation.[30] Because the amorphous TiO_2 has deep-level hole traps that reduce photocatalytic activity,[29] PSCs based on amorphous TiO_2 ETL show better stability than those based on anatase TiO_2 ETL.

Based on this observation, we wonder whether the direct contact between TiO_2 and $CH_3NH_3PbI_3$ is the cause for device

DOI: 10.1021/acs.jpcb.7b03921
J. Phys. Chem. B XXXX, XXX, XXX−XXX

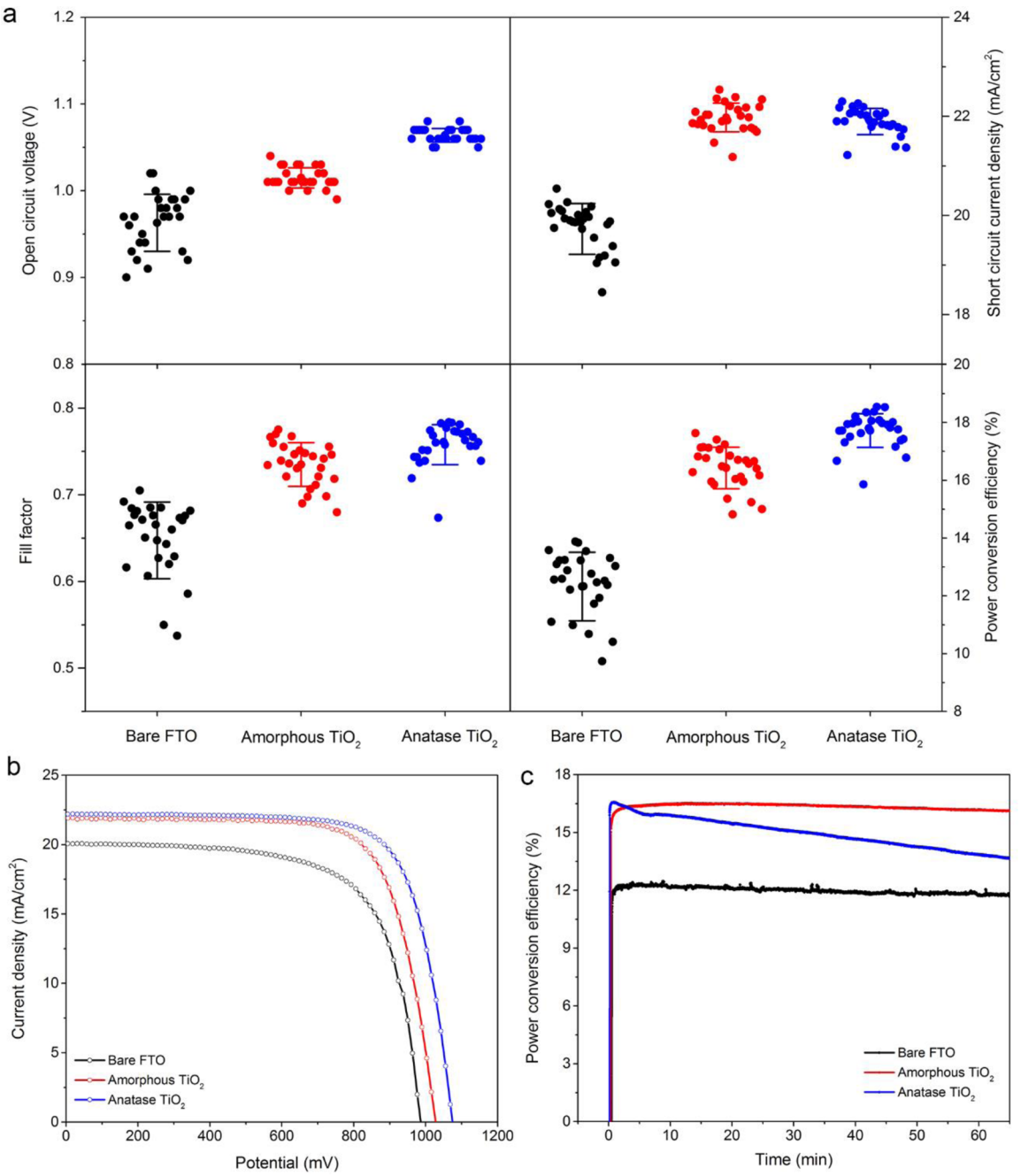

Figure 2. Solar cell performance on bare FTO, amorphous TiO_2 and anatase TiO_2. (a) V_{OC}, J_{SC}, FF, and PCE of 27 devices for each configuration. The devices were tested with a scan rate of 100 mV/s without preconditioning. (b) Typical $J-V$ curves and (c) PCE monitoring with MPPT for solar cells based bare FTO, amorphous TiO_2, and anatase TiO_2 ETL.

Table 1. Summary of the Photovoltaic Parameters Obtained from the Reverse Scan of the $J-V$ Curves

substrate	V_{OC} (V)	J_{SC} (mA/cm²)	FF (%)	PCE (%)
bare FTO	0.96 ± 0.03	19.7 ± 0.5	64.7 ± 4.4	12.3 ± 1.2
amorphous TiO_2	1.01 ± 0.01	22.0 ± 0.3	73.5 ± 2.5	16.4 ± 0.7
anatase TiO_2	1.06 ± 0.01	22.0 ± 0.3	75.8 ± 2.3	17.7 ± 0.6

instability, and how to modify the surface of TiO_2 to further increase the PCE and stability of PSCs. In this work, we propose to coat the TiO_2 surface with an interfacial layer to prevent the direct contact between TiO_2 and $CH_3NH_3PbI_3$. This strategy indeed leads to significantly improved stability of our devices. It is possible to use an inorganic interface blocking layer,[52] but the required complex process will limit its practical applications. In this study we introduce a thin layer of stable polymer to prevent the direct contact and interaction between TiO_2 and perovskite. Polymers with polar and nonpolar groups are chosen to illustrate how interface structure impact the PCE and stability of solar cells. PEIE and PEI are widely used surface modifier material for electronic devices, which consists of hydroxyl or amino groups to lower the work function of electrodes.[53] It has been successfully used in many organic devices, including working as cathode modifier in PSCs.[54,55] PS is a commonly used insulating polymer material and has been

DOI: 10.1021/acs.jpcb.7b03921
J. Phys. Chem. B XXXX, XXX, XXX−XXX

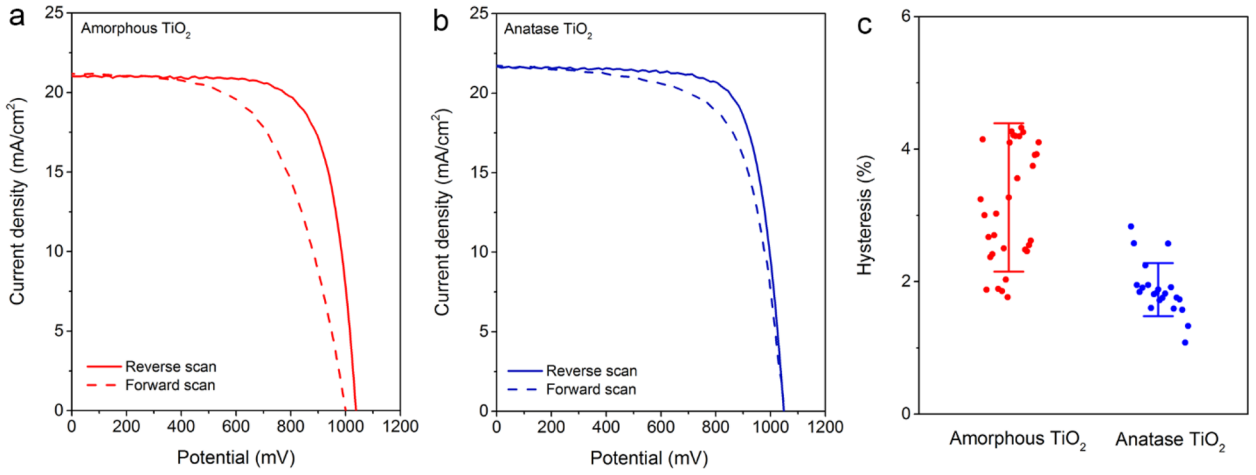

Figure 3. *J*–*V* curves by reverse and forward scan for devices based on (a) amorphous TiO_2 and (b) anatase TiO_2 substrates. (c) Hysteresis of solar cells based on amorphous TiO_2 and anatase TiO_2 substrates. The hysteresis is defined as the difference of PCE between reverse scan and forward scan.

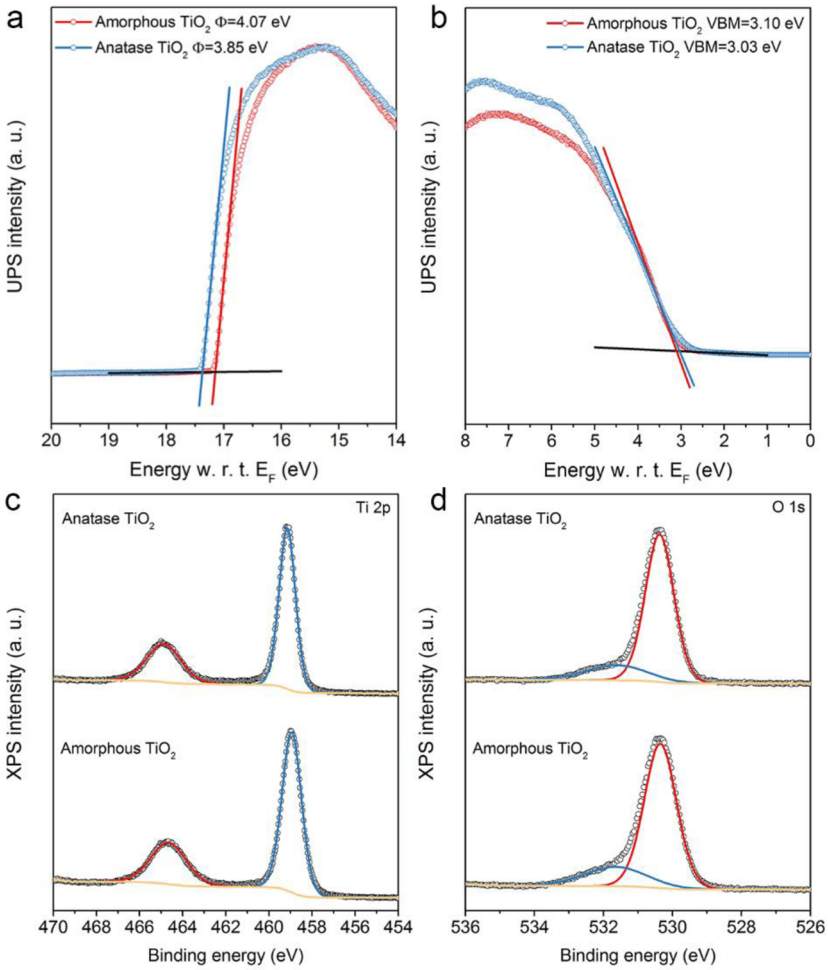

Figure 4. UPS/XPS of amorphous and anatase TiO_2 layers. (a) UPS (He–I) cutoff and (b) valence band spectrum in amorphous and anatase TiO_2 compact layer. (c) XPS (Al–Kα) Ti 2p core level spectrum and (d) O 1s core level spectrum of amorphous and anatase TiO_2 compact layer.

proposed as a potential alternative for PCBM, which is the electron transport material widely used in inverted structure perovskite solar cells.[33] These three polymers are stable in air and can be easily deposited by a solution spin-coating process. After coating with PEIE, PEI, or PS the transmittance of electrode has no observable change (Figure S3), indicating negligible absorption loss due to the additional modifier layer. The wettability of $CH_3NH_3PbI_3$ solution on amorphous TiO_2 and anatase TiO_2 was investigated (Figure S4). We find that amorphous TiO_2 has the poorer wettability compared with anatase TiO_2. After UV-Ozone treatment (which is part of perovskite solar cell device fabrication steps in this work), the

DOI: 10.1021/acs.jpcb.7b03921
J. Phys. Chem. B XXXX, XXX, XXX–XXX

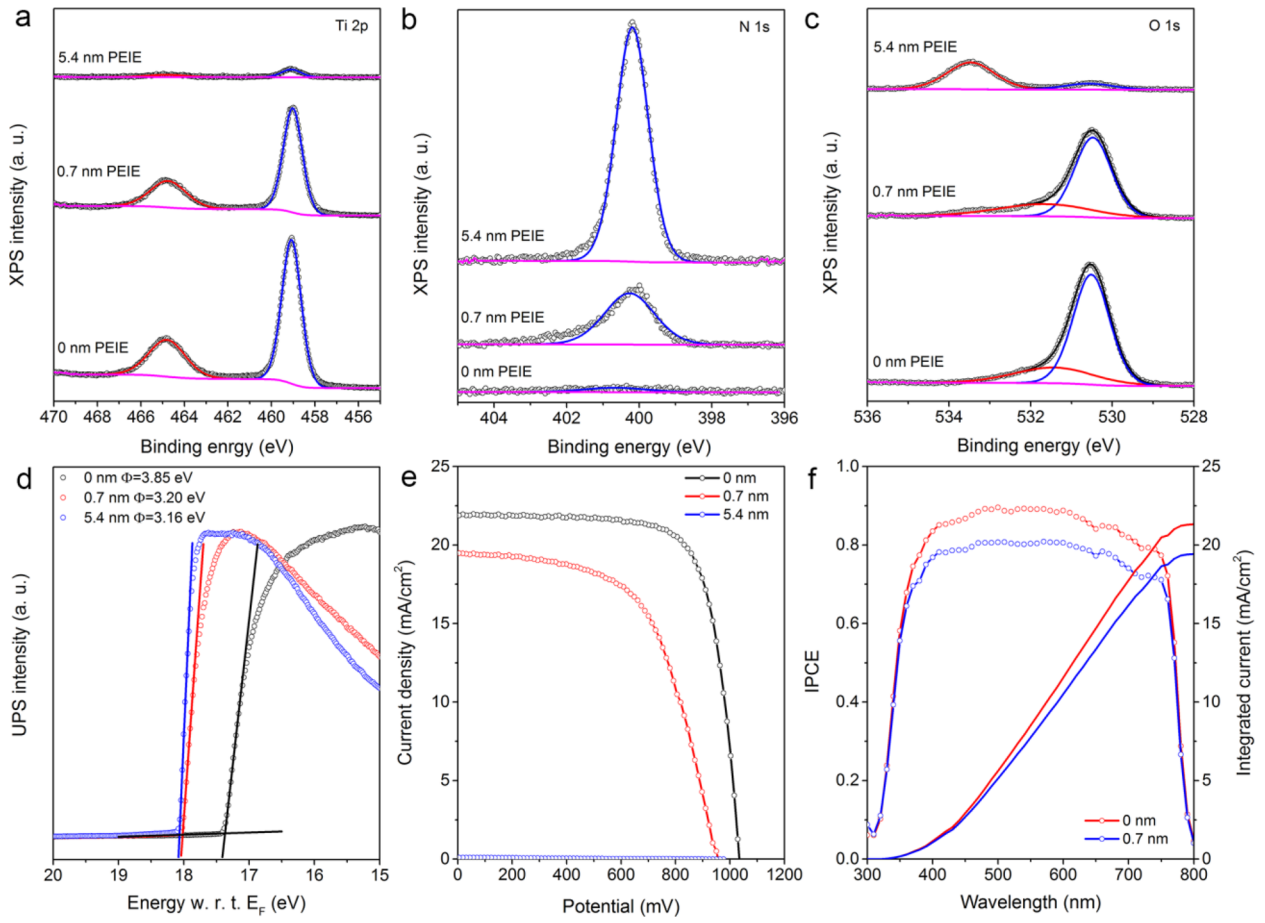

Figure 5. Photoemission spectroscopy measurement and solar cell performance with anatase TiO_2/PEIE bottom layer. (a) XPS (Al−Kα) Ti 2p, (b) N 1s, and (c) O 1s core level spectra of TiO_2/PEIE substrates with increasing thickness of PEIE. (d) UPS (He−I) cutoff of TiO_2/PEIE substrates with increasing thickness of PEIE. (e) and (f) Solar cell performance with different PEIE thickness on top of TiO_2.

wettability could be enhanced for both amorphous TiO_2 and anatase TiO_2. After coating PEIE, PEI, and PS the wettability of $CH_3NH_3PbI_3$ solution does not show much difference, with a little higher contact angle for PS interfacial layer (Figure S5). Overall, the wetting properties are similar for all substrates with different interfacial layers as well as UV-Ozone treated bare amorphous and anatase TiO_2, and therefore are expected to only have a weak influence on perovskite solar cell performance and stability.

Unlike previous reports,[54,55] here PEIE is chosen to both lower the work function of TiO_2 and prevent direct contact between TiO_2 and $CH_3NH_3PbI_3$. PEIE forms a uniform and full coverage film on the substrate (Figure S6). To confirm the presence of PEIE layer after deposition, we performed XPS measurements. We could clearly observe the N 1s peaks rising while the Ti 2p signal dropping with the increasing thickness of PEIE (Figures 5a,b). The two most significant features are the drastic decrease of the Ti−O signal (associated with the peak around 530.5 eV) and appearance of the H−O signal (associated with the peak around 533.5 eV) after increasing PEIE thickness (Figure 5c). The thickness of the PEIE layer is calculated based on XPS spectra,[56] which are similar to the reported results based on ellipsometry measurements.[55] Two thickness values (~0.7 and 5 nm) are investigated in this work. After the deposition of a thin PEIE layer, a decrease of ~0.7 eV in work function of the of FTO/TiO_2 electrode is observed based on the UPS measurements, suggesting the formation of an interface dipole (Figure 5d). Solar cell devices were fabricated using this FTO/TiO_2/PEIE substrate. Although we expect PCE and stability enhancement with this structure, the PCE of these solar cells is very low (Figure 5e,f). With only a 0.7 nm thick layer of PEIE, V_{OC}, J_{SC}, and FF all decrease (Figure S7). With 5 nm thick PEIE, almost no photovoltaic signal can be observed.

We observe no obvious difference between substrates based on XRD and absorbance measurements of $CH_3NH_3PbI_3$ (Figures S8−9). We propose that the deterioration of device performance after insertion of PEIE is caused by the interface interaction between polar PEIE molecules and $CH_3NH_3PbI_3$. One of the features of $CH_3NH_3PbI_3$ is the ionic structure. It has been reported recently that the surface modification of ETL with self-assembled monolayer (SAM) for PSCs is different from organic solar cells.[57] Due to the chemical interactions between SAM and perovskite, the PCE of PSCs is not enhanced as expected according to energy level alignment. To address this issue, we introduced another polymer PEI into the interface between TiO_2 and $CH_3NH_3PbI_3$. PEI is also a widely used material, which has rich amino groups to lower work function.[58] As illustrated in Figure S10a−c, with the increasing thickness of PEI layer, the amino group signal (associated with the peak around 400.5 eV in the N 1s core level spectrum) increases and the signals associated with the elements in the substrate (Ti and O) drastically decrease, which suggests a uniform coverage of PEI layer on TiO_2. Similar to the results

DOI: 10.1021/acs.jpcb.7b03921
J. Phys. Chem. B XXXX, XXX, XXX−XXX

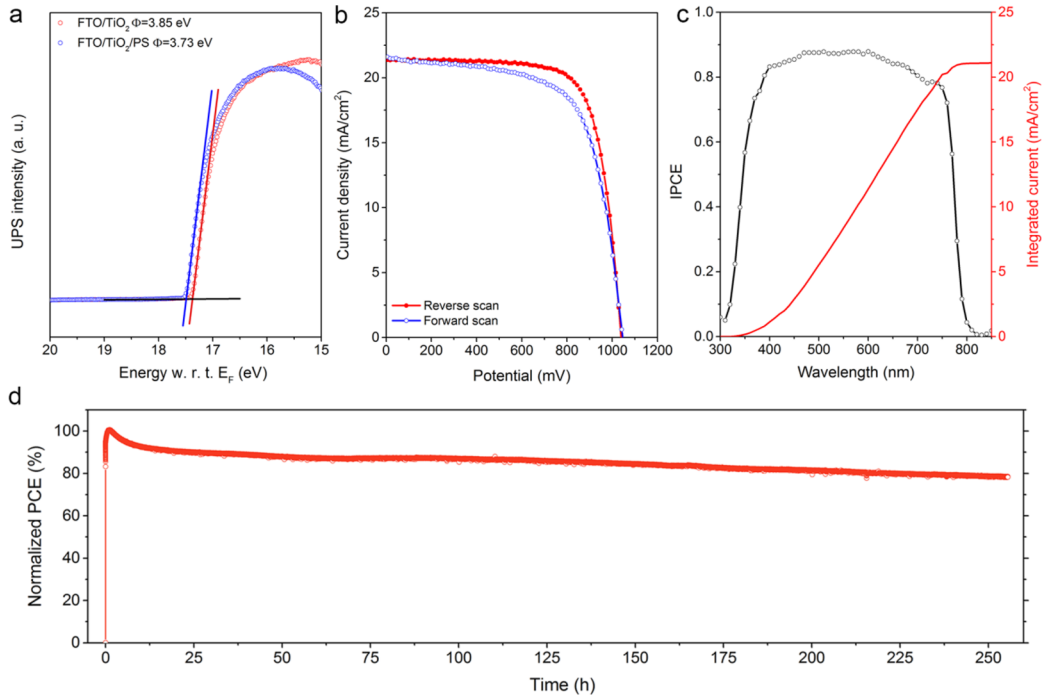

Figure 6. Solar cell performance with anatase TiO_2/PS bottom layer. (a) UPS (He–I) cutoff of FTO/TiO_2 and FTO/TiO_2/PS substrates. (b) Reverse and forward J–V curves. (c) IPCE and integrated short-circuit current density. (d) Maximum power point tracking under 5% RH box.

obtained with PEIE, the PCE of fabricated PSCs deteriorates with the PEI layer (Figure S10e). A decrease of ~1 eV of work function (Figure S10d) is also observed, suggesting the formation of dipole layer. This is consistent with the recently reported interaction between perovskite and SAM on top of SnO_2.[57] Our results imply that the presence of the interface dipole could induce band bending, leading to the band edge alignment shift and therefore deteriorating device performance.[42]

In contrast, the PS interface layer functions as a separation layer to prevent the interaction between TiO_2 and $CH_3NH_3PbI_3$. This insulating layer has been reported as the tunneling layer for electron transport.[33] PS forms an aromatic rich surface on top of TiO_2. We expect that only a weak van der Waals bond forms between the substrate and perovskite.[57] UPS measurements show that the PS layer lowers the work function of the FTO/TiO_2 substrate slightly (Figure 6a). This observation suggests no obvious formation of interface dipole at PS and perovskite interface, indicative of weak interface interaction. This is drastically different from the cases of PEIE and PEI. Solar cells with and without the PS insulating layer were fabricated and characterized. With an optimized process, the devices with PS exhibit PCE comparable to that of the anatase TiO_2 ETL (Figure 6b). A highest PCE of 17.1% is obtained. There is still small hysteresis possibly due to other factors such as ion migration in perovskite.[59,60] The IPCE of the device is approaching 88% and integrated J_{SC} (21.1 mA/cm^2) is consistent with recorded J–V curve (21.4 mA/cm^2) (Figure 6c). Expectedly, with this PS insulating layer the device shows enhanced stability both in air and dry conditions. With this PS interface layer, the devices degradation slow down significantly compared with the anatase TiO_2 substrate when measured in a 45% RH air (Figure S11). When recording the maximum power point output in a drybox with 5% RH the device shows a lifetime longer than 250 h (Figure 6d), which is even 4 times longer than amorphous TiO_2 compact layer based planar structure devices without an interfacial layer.

The morphology of the $CH_3NH_3PbI_3$ films on various underlying interfacial layers before and after thermal annealing was investigated. We find that before thermal annealing, the morphology of $CH_3NH_3PbI_3$ film is similar on various underlying interfacial layers with a high coverage (Figure S12). The morphology of the perovskites after the annealing treatment on the various underlying interfacial layers is provided in Figure S13. While after thermal annealing, both top-view surface morphology and cross-section view images clearly show that the morphology of $CH_3NH_3PbI_3$ is highly dependent on the underlying interfacial layers. With PEIE and PEI interfacial layers, the grain sizes of $CH_3NH_3PbI_3$ is much smaller compared to that on amorphous TiO_2, anatase TiO_2 and PS interfacial layer. This can be one of the main reasons why PEIE and PEI interfacial layers lead to low $CH_3NH_3PbI_3$ perovskite solar cells efficiencies. To address the influences of various underlying interfacial layers on the morphology of $CH_3NH_3PbI_3$ films, vacuum processes such as sequential vacuum deposition[61,62] and hybrid chemical vapor deposition process[46,63] can be a viable way to alleviate the strong dependence of the perovskite film morphology on underlying interfacial layers.

CONCLUSIONS

In this work we show that interface engineering can help improve the PCE and stability of PSCs. With $CH_3NH_3PbI_3$ as an active layer we show that PSCs based on crystalline anatase TiO_2 ETL show higher PCEs but poorer stability. PSCs based on amorphous TiO_2 ETL show improved stability but PCE is lower. Deposition of a thin interface layer of PS improves stability meanwhile maintaining the high performance. We show that the possible interface interactions between the thin interface layer and the perovskite film have a strong impact on

DOI: 10.1021/acs.jpcb.7b03921
J. Phys. Chem. B XXXX, XXX, XXX–XXX

device efficiency and stability. With insulating polymer PS as the interface layer on top of crystalline anatase TiO_2, the stability of solar cell is significantly improved and higher PCE is maintained. The lifetime of device with a PS layer is 4 times longer than PSCs based on unmodified amorphous TiO_2 ETL.

■ ASSOCIATED CONTENT

Supporting Information

The Supporting Information is available free of charge on the ACS Publications website at DOI: 10.1021/acs.jpcb.7b03921.

Maximum power point tracking of solar cells with amorphous TiO_2 compact layer and anatase TiO_2/PS bottom layer; transmittance spectra of FTO, FTO/TiO_2, FTO/TiO_2/PEIE, FTO/TiO_2/PEI, and FTO/TiO_2/PS substrate; SEM/EDS of PEIE layer on FTO substrate; contact angle of $CH_3NH_3PbI_3$ solution on different substrates; XRD spectra; UV−vis absorbance spectra and SEM of $CH_3NH_3PbI_3$ on different substrates; performance distribution of solar cells based on TiO_2/PEIE with PEIE film of 0.7 nm thickness; XPS results of PEI; and solar cell performance with anatase TiO_2/PEI bottom layer (PDF)

■ AUTHOR INFORMATION

Corresponding Author

*E-mail: Yabing.Qi@OIST.jp.

ORCID

Yabing Qi: 0000-0002-4876-8049

Notes

The authors declare no competing financial interest.

■ ACKNOWLEDGMENTS

This work was supported by funding from the Energy Materials and Surface Sciences Unit of the Okinawa Institute of Science and Technology Graduate University, the OIST R&D Cluster Research Program, the OIST Proof of Concept (POC) Program, and JSPS KAKENHI Grant Number 15K17925. We would like to thank Dr. Mikas Remeika for writing the software for steady state power measurements.

■ REFERENCES

(1) Kojima, A.; Teshima, K.; Shirai, Y.; Miyasaka, T. Organometal Halide Perovskites as Visible-Light Sensitizers for Photovoltaic Cells. *J. Am. Chem. Soc.* **2009**, *131*, 6050−6051.

(2) Yang, W. S.; Noh, J. H.; Jeon, N. J.; Kim, Y. C.; Ryu, S.; Seo, J.; Seok, S. I. High-Performance Photovoltaic Perovskite Layers Fabricated Through Intramolecular Exchange. *Science* **2015**, *348*, 1234−1237.

(3) Li, X.; Bi, D.; Yi, C.; Decoppet, J. D.; Luo, J.; Zakeeruddin, S. M.; Hagfeldt, A.; Gratzel, M. A Vacuum Flash-Assisted Solution Process for High-Efficiency Large-Area Perovskite Solar Cells. *Science* **2016**, *353*, 58−62.

(4) Wang, S.; Jiang, Y.; Juarez-Perez, E. J.; Ono, L. K.; Qi, Y. B. Accelerated Degradation of Methylammonium Lead Iodide Perovskites Induced by Exposure to Iodine Vapour. *Nat. Energy* **2016**, *2*, 16195.

(5) Jeon, N. J.; Noh, J. H.; Kim, Y. C.; Yang, W. S.; Ryu, S.; Seok, S. I. Solvent Engineering for High-Performance Inorganic-Organic Hybrid Perovskite Solar Cells. *Nat. Mater.* **2014**, *13*, 897−903.

(6) Jeon, N. J.; Noh, J. H.; Yang, W. S.; Kim, Y. C.; Ryu, S.; Seo, J.; Seok, S. I. Compositional Engineering of Perovskite Materials for High-Performance Solar Cells. *Nature* **2015**, *517*, 476−480.

(7) Saliba, M.; Matsui, T.; Seo, J. Y.; Domanski, K.; Correa-Baena, J. P.; Nazeeruddin, M. K.; Zakeeruddin, S. M.; Tress, W.; Abate, A.; Hagfeldt, A.; et al. Cesium-Containing Triple Cation Perovskite Solar Cells: Improved Stability, Reproducibility and High Efficiency. *Energy Environ. Sci.* **2016**, *9*, 1989−1997.

(8) Saliba, M.; Matsui, T.; Domanski, K.; Seo, J. Y.; Ummadisingu, A.; Zakeeruddin, S. M.; Correa-Baena, J. P.; Tress, W. R.; Abate, A.; Hagfeldt, A.; et al. Incorporation of Rubidium Cations into Perovskite Solar Cells Improves Photovoltaic Performance. *Science* **2016**, *354*, 206−209.

(9) Kato, Y.; Ono, L. K.; Lee, M. V.; Wang, S.; Raga, S. R.; Qi, Y. B. Silver Iodide Formation in Methyl Ammonium Lead Iodide Perovskite Solar Cells with Silver Top Electrodes. *Adv. Mater. Interfaces* **2015**, *2*, 1500195.

(10) Hawash, Z.; Ono, L. K.; Raga, S. R.; Lee, M. V.; Qi, Y. B. Air-Exposure Induced Dopant Redistribution and Energy Level Shifts in Spin-Coated Spiro-MeOTAD Films. *Chem. Mater.* **2015**, *27*, 562−569.

(11) Ono, L. K.; Raga, S. R.; Remeika, M.; Winchester, A. J.; Gabe, A.; Qi, Y. B. Pinhole-Free Hole Transport Layers Significantly Improve the Stability of $MAPbI_3$-Based Perovskite Solar Cells under Operating Conditions. *J. Mater. Chem. A* **2015**, *3*, 15451−15456.

(12) Jung, M. C.; Raga, S. R.; Ono, L. K.; Qi, Y. B. Substantial Improvement of Perovskite Solar Cells Stability by Pinhole-Free Hole Transport Layer with Doping Engineering. *Sci. Rep.* **2015**, *5*, 9863.

(13) Yang, J.; Siempelkamp, B. D.; Mosconi, E.; De Angelis, F.; Kelly, T. L. Origin of the Thermal Instability in $CH_3NH_3PbI_3$Thin Films Deposited on ZnO. *Chem. Mater.* **2015**, *27*, 4229−4236.

(14) Dkhissi, Y.; Meyer, S.; Chen, D.; Weerasinghe, H. C.; Spiccia, L.; Cheng, Y. B.; Caruso, R. A. Stability Comparison of Perovskite Solar Cells Based on Zinc Oxide and Titania on Polymer Substrates. *ChemSusChem* **2016**, *9*, 687−695.

(15) Ono, L. K.; Qi, Y. B. Surface and Interface Aspects of Organometal Halide Perovskite Materials and Solar Cells. *J. Phys. Chem. Lett.* **2016**, *7*, 4764−4794.

(16) Ahn, N.; Kwak, K.; Jang, M. S.; Yoon, H.; Lee, B. Y.; Lee, J. K.; Pikhitsa, P. V.; Byun, J.; Choi, M. Trapped Charge-Driven Degradation of Perovskite Solar Cells. *Nat. Commun.* **2016**, *7*, 13422.

(17) van Reenen, S.; Kemerink, M.; Snaith, H. J. Modeling Anomalous Hysteresis in Perovskite Solar Cells. *J. Phys. Chem. Lett.* **2015**, *6*, 3808−3814.

(18) Calado, P.; Telford, A. M.; Bryant, D.; Li, X.; Nelson, J.; O'Regan, B. C.; Barnes, P. R. Evidence for Ion Migration in Hybrid Perovskite Solar Cells with Minimal Hysteresis. *Nat. Commun.* **2016**, *7*, 13831.

(19) Yang, Y.; Yang, M.; Moore, D. T.; Yan, Y.; Miller, E. M.; Zhu, K.; Beard, M. C. Top and Bottom Surfaces Limit Carrier Lifetime in Lead Iodide Perovskite Films. *Nat. Energy* **2017**, *2*, 16207.

(20) Yang, G.; Tao, H.; Qin, P.; Ke, W.; Fang, G. Recent Progress in Electron Transport Layers for Efficient Perovskite Solar Cells. *J. Mater. Chem. A* **2016**, *4*, 3970−3990.

(21) Snaith, H. J.; Abate, A.; Ball, J. M.; Eperon, G. E.; Leijtens, T.; Noel, N. K.; Stranks, S. D.; Wang, J. T.; Wojciechowski, K.; Zhang, W. Anomalous Hysteresis in Perovskite Solar Cells. *J. Phys. Chem. Lett.* **2014**, *5*, 1511−1515.

(22) Yang, D.; Zhou, X.; Yang, R.; Yang, Z.; Yu, W.; Wang, X.; Li, C.; Liu, S.; Chang, R. P. H. Surface Optimization to Eliminate Hysteresis for Record Efficiency Planar Perovskite Solar Cells. *Energy Environ. Sci.* **2016**, *9*, 3071−3078.

(23) Giordano, F.; Abate, A.; Correa Baena, J. P.; Saliba, M.; Matsui, T.; Im, S. H.; Zakeeruddin, S. M.; Nazeeruddin, M. K.; Hagfeldt, A.; Graetzel, M. Enhanced Electronic Properties in Mesoporous TiO_2 via Lithium Doping for High-Efficiency Perovskite Solar Cells. *Nat. Commun.* **2016**, *7*, 10379.

(24) Zhang, H.; Shi, J.; Xu, X.; Zhu, L.; Luo, Y.; Li, D.; Meng, Q. Mg-Doped TiO_2 Boosts the Efficiency of Planar Perovskite Solar Cells to Exceed 19%. *J. Mater. Chem. A* **2016**, *4*, 15383−15389.

(25) Tan, H.; Jain, A.; Voznyy, O.; Lan, X.; Garcia de Arquer, F. P.; Fan, J. Z.; Quintero-Bermudez, R.; Yuan, M.; Zhang, B.; Zhao, Y.; et al.

Efficient and Stable Solution-Processed Planar Perovskite Solar Cells via Contact Passivation. *Science* **2017**, *355*, 722−726.
(26) Dong, Q.; Shi, Y.; Wang, K.; Li, Y.; Wang, S.; Zhang, H.; Xing, Y.; Du, Y.; Bai, X.; Ma, T. Insight into Perovskite Solar Cells Based on SnO_2 Compact Electron-Selective Layer. *J. Phys. Chem. C* **2015**, *119*, 10212−10217.
(27) Shao, Y.; Xiao, Z.; Bi, C.; Yuan, Y.; Huang, J. Origin and Elimination of Photocurrent Hysteresis by Fullerene Passivation in $CH_3NH_3PbI_3$ Planar Heterojunction Solar Cells. *Nat. Commun.* **2014**, *5*, 5784.
(28) Son, D.-Y.; Im, J.-H.; Kim, H.-S.; Park, N.-G. 11% Efficient Perovskite Solar Cell Based on ZnO Nanorods: An Effective Charge Collection System. *J. Phys. Chem. C* **2014**, *118*, 16567−16573.
(29) Li, Y.; Cooper, J. K.; Liu, W.; Sutter-Fella, C. M.; Amani, M.; Beeman, J. W.; Javey, A.; Ager, J. W.; Liu, Y.; Toma, F. M.; et al. Defective TiO_2 with High Photoconductive Gain for Efficient and Stable Planar Heterojunction Perovskite Solar Cells. *Nat. Commun.* **2016**, *7*, 12446.
(30) Leijtens, T.; Eperon, G. E.; Pathak, S.; Abate, A.; Lee, M. M.; Snaith, H. J. Overcoming Ultraviolet Light Instability of Sensitized TiO_2 with Meso-Superstructured Organometal Tri-Halide Perovskite Solar Cells. *Nat. Commun.* **2013**, *4*, 2885.
(31) Lee, S. W.; Kim, S.; Bae, S.; Cho, K.; Chung, T.; Mundt, L. E.; Lee, S.; Park, S.; Park, H.; Schubert, M. C.; et al. UV Degradation and Recovery of Perovskite Solar Cells. *Sci. Rep.* **2016**, *6*, 38150.
(32) Bella, F.; Griffini, G.; Correa-Baena, J. P.; Saracco, G.; Gratzel, M.; Hagfeldt, A.; Turri, S.; Gerbaldi, C. Improving Efficiency and Stability of Perovskite Solar Cells with Photocurable Fluoropolymers. *Science* **2016**, *354*, 203−206.
(33) Wang, Q.; Dong, Q.; Li, T.; Gruverman, A.; Huang, J. Thin Insulating Tunneling Contacts for Efficient and Water-Resistant Perovskite Solar Cells. *Adv. Mater.* **2016**, *28*, 6734−6739.
(34) Ahn, N.; Son, D. Y.; Jang, I. H.; Kang, S. M.; Choi, M.; Park, N. G. Highly Reproducible Perovskite Solar Cells with Average Efficiency of 18.3% and Best Efficiency of 19.7% Fabricated via Lewis Base Adduct of Lead(II) Iodide. *J. Am. Chem. Soc.* **2015**, *137*, 8696−8699.
(35) Son, D.-Y.; Lee, J.-W.; Choi, Y. J.; Jang, I.-H.; Lee, S.; Yoo, P. J.; Shin, H.; Ahn, N.; Choi, M.; Kim, D.; et al. Self-Formed Grain Boundary Healing Layer for Highly Efficient $CH_3NH_3PbI_3$ Perovskite Solar Cells. *Nat. Energy* **2016**, *1*, 16081.
(36) Raga, S. R.; Qi, Y. B. The Effect of Impurities on the Impedance Spectroscopy Response of $CH_3NH_3PbI_3$ Perovskite Solar Cells. *J. Phys. Chem. C* **2016**, *120*, 28519−28526.
(37) Liu, D.; Yang, J.; Kelly, T. L. Compact Layer Free Perovskite Solar Cells with 13.5% Efficiency. *J. Am. Chem. Soc.* **2014**, *136*, 17116−17122.
(38) Ke, W.; Fang, G.; Wan, J.; Tao, H.; Liu, Q.; Xiong, L.; Qin, P.; Wang, J.; Lei, H.; Yang, G.; et al. Efficient Hole-Blocking Layer-Free Planar Halide Perovskite Thin-Film Solar Cells. *Nat. Commun.* **2015**, *6*, 6700.
(39) Qiu, L.; He, S.; Yang, J.; Deng, J.; Peng, H. Fiber-Shaped Perovskite Solar Cells with High Power Conversion Efficiency. *Small* **2016**, *12*, 2419−2424.
(40) Yang, D.; Yang, R.; Zhang, J.; Yang, Z.; Liu, S.; Li, C. High Efficiency Flexible Perovskite Solar Cells Using Superior Low Temperature TiO_2. *Energy Environ. Sci.* **2015**, *8*, 3208−3214.
(41) Tang, H.; Prasad, K.; Sanjinès, R.; Schmid, P. E.; Lévy, F. Electrical and Optical Properties of TiO_2 Anatase Thin Films. *J. Appl. Phys.* **1994**, *75*, 2042−2047.
(42) Geng, W.; Tong, C. J.; Liu, J.; Zhu, W.; Lau, W. M.; Liu, L. M. Structures and Electronic Properties of Different $CH_3NH_3PbI_3/TiO_2$ Interface: A First-Principles Study. *Sci. Rep.* **2016**, *6*, 20131.
(43) Yella, A.; Heiniger, L. P.; Gao, P.; Nazeeruddin, M. K.; Gratzel, M. Nanocrystalline Rutile Electron Extraction Layer Enables Low-Temperature Solution Processed Perovskite Photovoltaics with 13.7% Efficiency. *Nano Lett.* **2014**, *14*, 2591−2596.
(44) Anaraki, E. H.; Kermanpur, A.; Steier, L.; Domanski, K.; Matsui, T.; Tress, W.; Saliba, M.; Abate, A.; Grätzel, M.; Hagfeldt, A.; et al. Highly Efficient and Stable Planar Perovskite Solar Cells by Solution-Processed Tin Oxide. *Energy Environ. Sci.* **2016**, *9*, 3128−3134.
(45) Yang, D.; Yang, Z.; Qin, W.; Zhang, Y.; Liu, S.; Li, C. Alternating Precursor Layer Deposition for Highly Stable Perovskite Films Towards Efficient Solar Cells Using Vacuum Deposition. *J. Mater. Chem. A* **2015**, *3*, 9401−9405.
(46) Leyden, M. R.; Lee, M. V.; Raga, S. R.; Qi, Y. B. Large Formamidinium Lead Trihalide Perovskite Solar Cells Using Chemical Vapor Deposition with High Reproducibility and Tunable Chlorine Concentrations. *J. Mater. Chem. A* **2015**, *3*, 16097−16103.
(47) Nowotny, M. K.; Bak, T.; Nowotny, J. Electrical Properties and Defect Chemistry of TiO_2 Single Crystal. I. Electrical Conductivity. *J. Phys. Chem. B* **2006**, *110*, 16270−16282.
(48) Wojciechowski, K.; Saliba, M.; Leijtens, T.; Abate, A.; Snaith, H. J. Sub-150 °C Processed Meso-Superstructured Perovskite Solar Cells with Enhanced Efficiency. *Energy Environ. Sci.* **2014**, *7*, 1142−1147.
(49) Chen, W.; Wu, Y.; Yue, Y.; Liu, J.; Zhang, W.; Yang, X.; Chen, H.; Bi, E.; Ashraful, I.; Gratzel, M.; et al. Efficient and Stable Large-Area Perovskite Solar Cells with Inorganic Charge Extraction Layers. *Science* **2015**, *350*, 944−948.
(50) Schulz, P.; Edri, E.; Kirmayer, S.; Hodes, G.; Cahen, D.; Kahn, A. Interface Energetics in Organo-Metal Halide Perovskite-Based Photovoltaic cells. *Energy Environ. Sci.* **2014**, *7*, 1377−1381.
(51) Fan, C.; Chen, C.; Wang, J.; Fu, X.; Ren, Z.; Qian, G.; Wang, Z. Black Hydroxylated Titanium Dioxide Prepared via Ultrasonication with Enhanced Photocatalytic Activity. *Sci. Rep.* **2015**, *5*, 11712.
(52) Ito, S.; Tanaka, S.; Manabe, K.; Nishino, H. Effects of Surface Blocking Layer of Sb_2S_3 on Nanocrystalline TiO_2 for $CH_3NH_3PbI_3$ Perovskite Solar Cells. *J. Phys. Chem. C* **2014**, *118*, 16995−17000.
(53) Zhou, Y.; Fuentes-Hernandez, C.; Shim, J.; Meyer, J.; Giordano, A. J.; Li, H.; Winget, P.; Papadopoulos, T.; Cheun, H.; Kim, J.; et al. A Universal Method to Produce Low-Work Function Electrodes for Organic Electronics. *Science* **2012**, *336*, 327−332.
(54) Zhou, H.; Chen, Q.; Li, G.; Luo, S.; Song, T. B.; Duan, H. S.; Hong, Z.; You, J.; Liu, Y.; Yang, Y. Interface Engineering of Highly Efficient Perovskite Solar Cells. *Science* **2014**, *345*, 542−546.
(55) Song, S.; Moon, B. J.; Hörantner, M. T.; Lim, J.; Kang, G.; Park, M.; Kim, J. Y.; Snaith, H. J.; Park, T. Interfacial Electron Accumulation for Efficient Homo-Junction Perovskite Solar Cells. *Nano Energy* **2016**, *28*, 269−276.
(56) Gunter, P. L. J.; De Jong, A. M.; Niemantsverdriet, J. W.; Rheiter, H. J. H. Evaluation of Take-off-Angle-Dependent XPS for Determining the Thickness of Passivation Layers on Aluminium and Silicon. *Surf. Interface Anal.* **1992**, *19*, 161−164.
(57) Zuo, L.; Chen, Q.; De Marco, N.; Hsieh, Y. T.; Chen, H.; Sun, P.; Chang, S. Y.; Zhao, H.; Dong, S.; Yang, Y. Tailoring the Interfacial Chemical Interaction for High-Efficiency Perovskite Solar Cells. *Nano Lett.* **2017**, *17*, 269−275.
(58) Liao, H.-C.; Guo, P.; Hsu, C.-P.; Lin, M.; Wang, B.; Zeng, L.; Huang, W.; Soe, C. M. M.; Su, W.-F.; Bedzyk, M. J.; et al. Enhanced Efficiency of Hot-Cast Large-Area Planar Perovskite Solar Cells/Modules Having Controlled Chloride Incorporation. *Adv. Energy Mater.* **2017**, *7*, 1601660.
(59) Leguy, A. M.; Frost, J. M.; McMahon, A. P.; Sakai, V. G.; Kochelmann, W.; Law, C.; Li, X.; Foglia, F.; Walsh, A.; O'Regan, B. C.; et al. The Dynamics of Methylammonium Ions in Hybrid Organic-Inorganic Perovskite Solar Cells. *Nat. Commun.* **2015**, *6*, 7124.
(60) Bag, M.; Renna, L. A.; Adhikari, R. Y.; Karak, S.; Liu, F.; Lahti, P. M.; Russell, T. P.; Tuominen, M. T.; Venkataraman, D. Kinetics of Ion Transport in Perovskite Active Layers and Its Implications for Active Layer Stability. *J. Am. Chem. Soc.* **2015**, *137*, 13130−13137.
(61) Burschka, J.; Pellet, N.; Moon, S. J.; Humphry-Baker, R.; Gao, P.; Nazeeruddin, M. K.; Gratzel, M. Sequential Deposition as a Route to High-Performance Perovskite-Sensitized Solar Cells. *Nature* **2013**, *499*, 316−319.
(62) Ono, L. K.; Wang, S.; Kato, Y.; Raga, S. R.; Qi, Y. B. Fabrication of Semi-Transparent Perovskite Films with Centimeter-Scale Superior Uniformity by the Hybrid Deposition Method. *Energy Environ. Sci.* **2014**, *7*, 3989−3993.

DOI: 10.1021/acs.jpcb.7b03921
J. Phys. Chem. B XXXX, XXX, XXX−XXX

(63) Leyden, M. R.; Ono, L. K.; Raga, S. R.; Kato, Y.; Wang, S.; Qi, Y. B. High Performance Perovskite Solar Cells by Hybrid Chemical Vapor Deposition. *J. Mater. Chem. A* **2014**, *2*, 18742−18745.

DOI: 10.1021/acs.jpcb.7b03921
J. Phys. Chem. B XXXX, XXX, XXX−XXX